A dual-functional wave-power plant for wave-energy extraction and shore protection: A wave-flume study

Conghao Xu[a], Zhenhua Huang[a,*]

[a]*Department of Ocean and Resources Engineering, School of Ocean and Earth Science and Technology, University of Hawaii at Manoa, Honolulu HI 96822 USA*

Abstract

The fundamental roadblock toward commercial-scale wave power operations is cost. The main objective of this work was to address the cost challenge facing wave energy commercialization through cost-sharing with pile breakwaters to be built for shore protection. This was achieved in this study through a dual-functional wave-power plant for generation of wave-power electricity and protection against coastal erosion for sustainable coastal development. The dual-functional wave-power plant was formed by integrating oscillating-water-column (OWC) devices into a pile breakwater, with each pile being an OWC-pile equipped with a power take-off device. The power extraction efficiency and hydrodynamic characteristics of the dual-functional wave-power plant were measured in a wave flume under various wave conditions. An orifice was used at the top of the pneumatic chamber of each OWC-pile to simulate the power take-off device. To evaluate the performance of the power plant in wave power extraction and shore protection, the surface elevation and pressure inside the OWC chamber, as well as the scattered waves, were measured. It was found that comparing to a standalone OWC-pile device with an identical design and geometric characteristics, an OWC-pile in the dual-functional wave-power plant could achieve significantly larger power-extraction efficiency. Comparing to a pile breakwater with the same dimensions, the wave transmission and reflection of the dual-functional wave-power plant were both weaker, especially the wave reflection, which is beneficial for structure safety and shore protection. Based on the Froude's law of similarity and an estimation of the effect of air compressibility at full scale, an evaluation of the performance of a dual-functional wave-power plant at full scale was also provided. The findings of this work promote close collaboration between wave-energy utilization community and the shore-protection community for commercial-scale deployment of wave energy converters and contribute to making wave energy economically competitive.

Keywords: wave farm; marine renewable energy; oscillating water column; pile breakwater; vortex shedding; shore protection

*Corresponding author contacts:
Email address: zhenhua@hawaii.edu (Zhenhua Huang)

1. Introduction

With the increase of global energy demand and a rising concern of the environmental consequences of fossil fuel based energy sources, the global need for clean and renewable energy is on the rise over the last decades. Taking Hawaii as an example, the state is surrounded by the Pacific Ocean, and a core strategic goal of its energy policy is to maximize affordable clean energy. The state has determined to achieve 100 percent renewable energy generation by 2045 (Hawaii State Energy Office, 2007). The ocean is a tremendous source of renewable energy, and ocean wave energy is one of the four main sources of energy in the ocean: the available ocean wave energy is on the terawatt level (Falnes, 2007; Bureau of Ocean Energy Management, 2017).

Among all Wave-Energy-Conversion (WEC) devices studied so far, Oscillating-Water-Column (OWC) type devices are one of the most studied and tested WEC devices. A typical OWC device usually consists of a semi-closed and semi-submerged pneumatic chamber and a power take-off (PTO) system (i.e., a turbine and an electric generator). Incident waves create a fluctuation of the air pressure inside the pneumatic chamber, which forces the air trapped in the chamber to drive a turbine connected to a generator for electricity generation (Evans, 1978).

Experimental, theoretical and numerical studies of OWC devices have been carried out in the past decades. Most of the existing studies are for standalone OWC devices, aiming mainly at improving their conversion efficiencies. Using linear wave theory, Evans (1978) found that it was possible to extract wave energy from ocean waves through the resonant interaction between water waves and a pneumatic chamber, and thus laid the foundation to the theories of hydrodynamics of OWC devices. Subsequent theoretical studies considered spatial non-uniformity of the water surface (Evans, 1982) and the compressibility of the air (Sarmento and Falcao, 1985) inside the OWC chamber. Most experimental studies on standalone OWC devices focused on the conversion efficiency of various designs. Bingham et al. (2015) performed a numerical and laboratory study of a 40-chamber I-beam attenuator in fixed and floating conditions and obtained a good agreement between their experiment and numerical results. Iturrioz et al. (2015) studied, experimentally and numerically, a simple shore mounted OWC device with a rectangular pneumatic chamber and showed a good agreement between their experimental results and numerical predictions. Ning et al. (2016b) studied experimentally the wave energy conversion efficiency, as well as the related hydrodynamics, of a fixed oscillating water column device with a 2D rectangular cross-section under various wave conditions and geometric parameters; their experimental results agreed well with previous numerical results obtained by a nonlinear potential-flow solver (Ning et al., 2015). Ning et al. (2016a) applied the numerical model of Ning et al. (2015) to investigate the dynamic wave forces on a 2D rectangular OWC device under various wave conditions and showed a good agreement between the experimental and numerical results. (Fleming and Macfarlane,

2017; Vyzikas et al., 2017) investigated experimentally how the underwater geometry could affect the energy loss and conversion efficiency of an OWC device. Fleming and Macfarlane (2017) carried out 2D PIV experiments that measure the detailed flow field in a 2D rectangular OWC chamber and used it to investigate the energy loss and conversion efficiency of OWC device with different underwater geometries; of all the geometries tested, it was hard to determine a best overall performance, and recommendations were made for future design of geometry. Vyzikas et al. (2017) conducted laboratory experiment with and without PTO mechanism for a series of geometric modifications to the classic design of OWC and the U-OWC devices, shape improvement suggestions were made according to the experimental results; they found that adding a slope in the chamber could improve the performance of the U-OWC device, while a small toe protection unit could enhance the performance of a classic OWC device. Prototype tests of OWC devices have also been carried out in Portugal, Norway, China, and India (Falcao, 2000; Zhang et al., 2009).

The methods used for numerical time-domain studies related to OWC devices can generally be categorized into two types: non-linear potential solvers and computational fluid dynamics (CFD) models. Koo and Kim (2010) used a nonlinear potential solver to study the performance and motion responses of OWC devices in wave fields; their solver was based on a fully non-linear boundary element method combined with a mixed Eulerian-Lagrangian method. Using a time-domain higher-order boundary element method (HOBEM), Ning et al. (2015) developed a 2D fully non-linear numerical wave flume to study the performance of a fixed OWC device; their numerical wave flume was validated against the experimental results reported in Ning et al. (2016b,a). Computational fluid dynamics (CFD) models, which solve Navier-Stokes equations and various turbulence closures, are computationally costly, but can capture viscous phenomena such as viscous dissipation and generation of vorticity. Zhang et al. (2012) developed a numerical method based on a two-phase level set and immersed boundary method and Navier-Stokes equation using FLUENT software, and the model validation against the existing experimental results showed a satisfactory agreement in terms of the oscillation of the free surface inside the chamber and the power extraction efficiency. To study the influence of OWC chamber geometry and turbine characteristics on OWC device performance, an aerodynamic model for the air pressure inside the OWC chamber was included in the CFD simulation of Teixeira et al. (2013). Iturrioz et al. (2015) and Simonetti et al. (2015) used the open source C++ CFD library OpenFOAM® to study hydrodynamics and wave-energy conversion of OWC devices and highlighted the capability of OpenFOAM® to accurately simulate important physical processes involved in the energy conversion of OWC devices. More recently, Elhanafi et al. (2016a, 2017) used the CFD software package StarCCM® to investigate hydrodynamics and energy conversion of two OWC devices with 2D rectangular OWC chambers (a tension-leg type floating-moored OWC device and a fixed OWC device with different lip shapes) and yielded good agreements with the measured energy conversion and motion responses.

Even though power from ocean waves can potentially make a significant contribu-

tion as a renewable energy source, a host of challenges, including high costs incurred in using the current technologies to generate electricity(López et al., 2013), have made the electricity generated by wave energy devices economically less competitive. These challenges include reducing construction and operation costs, increasing reliability, being suitable for a wide range of wave conditions, and minimizing potential environmental impacts. For example, while a WEC device must be optimized to the local prevailing wave conditions, its structure must withstand local extreme events, which will significantly increase the construction and maintenance costs of wave-power plants. To make wave energy economically competitive, innovative concepts to reduce costs are crucial in order to overcome the cost hurdle associated with wave energy utilization. Combining wave extraction with shore protection is one potential route to take.

Even though several studies have proposed the concept of integrating WECs with caisson or rubble mound or vertical wall breakwaters, these studies do not focus on shore protection and minimizing potential environmental impacts on coastal water quality. For example, the prototype project that integrated an overtopping-type WEC with a rubble mound breakwater at the port of Naples in Italy (Vicinanza et al., 2013; Contestabile et al., 2016) was not designed for shore protection; Yueh and Chuang (2013) proposed an integration of a piston-type porous wave energy converter into a vertical wall breakwater, but vertical walls do not allow water exchange across the breakwater and thus may have potential negative environmental impacts. Integration of OWCs with caisson breakwaters have been reported by several authors. Martins-Rivas and Mei (2009) and Henriques et al. (2013) studied the integration of a single OWC at the tip of a vertical wall, focusing on the influence of the vertical breakwater on the power-extraction efficiency of the OWC device. A wave power plant consisting of 16 OWC-chambers built into a caisson breakwater was constructed at the port of Mutriku, Spain (Torre-Enciso et al., 2009). Boccotti (2007a), Boccotti et al. (2007) and Boccotti (2007b) studied theoretically and experimentally a caisson breakwater with a U-OWC device with its power take-off modeled as a small opening; they showed that by properly optimizing the design of the caisson breakwater-OWC system, the efficiency of the U-OWC device could be greatly improved. A prototype caisson breakwater with a U-OWC was later constructed in the Mediterranean Sea in REWEC3 project (Arena et al., 2013) at the harbor of Civitavecchia, Italy. Because of the large hydrodynamic loads, caisson breakwaters are usually constructed in relatively shallow water on rubble mound foundations with armor layers. Various sources of wave energy dissipation inevitably reduce the amount of energy that can reach the OWC devices embodied in the caisson (Mustapa et al., 2017). Moreover, as an impermeable structure, a caisson type OWC-breakwater does not allow water, marine life and sediment exchange across it, which may potentially introduce high ecological footprint.

Most of the coastal structures that have been considered in the aforementioned studies are constructed either onshore or inside the surf zone. Since wave breaking will dissipate wave energy significantly and thus reduce the available wave energy reaching

shore-based wave power plants, it is desirable to deploy the OWC devices offshore just outside the surf zone. Generally speaking, full-scale studies on integrating OWCs with breakwaters other than caisson or rubble mound breakwaters are still lacking (Mustapa et al., 2017). For a more detailed review on existing effort to integrate WEC devices with breakwaters, the reader is referred to Mustapa et al. (2017).

Even though the concept of using an array of floating WECs for shore protection has been explored through numerical simulations, there is still a lack of model test results in the literature. For example, the idea of using offshore wave farms for shore protection has been explored recently by Abanade et al. (2014) and Mendoza et al. (2014). They studied loosely-spaced floating WECs and found that the wave farms might reduce erosion at the beach face through the reduction of wave transmission by an array of WECs. The applicability of the numerical methods used in these studies is crucially dependent on the parametrization of wave-energy loss due to WECs, which can only be obtained through physical model tests. Furthermore, mooring-line design and durability are two important issues for the safe operation of floating structures–to ensure the safety of floating OWCs in local extreme events, costs incurred in implementing these concepts will go up. Stratigaki et al. (2015) experimentally studied an array of 25 heaving buoys and found a significant effect on wave activity on the down-wave side of the array; however, allowing the wave buoys to move in just heave mode is a challenge in practice (e.g., effect of biofouling on the heave motion, large friction loss, high requirement on its structural strength). In terms of safety and maintenance costs, it may be preferable to use bottom-sitting fixed WECs such as pile-type OWCs, which can be easily constructed outside the surf zone to make more wave energy available for extraction. The authors are not aware of other experimental studies of bottom-sitting wave farm concepts in the literature, aiming at wave power-extraction as well as shore protection.

Pile breakwaters are shore-parallel structures, which have been traditionally used at small boat harbors or marinas. A typical pile breakwater consists of a row of closely-spaced piles (Kakuno and Liu, 1993; Sundar et al., 2002; Suh et al., 2007). Compared to traditional bottom-sitting breakwaters, the construction and maintenance costs of pile breakwaters are relatively insensitive to water depth, allowing such structures to be built deeper outside the surf zone. Compared to floating moored and pile-supported breakwaters, pile breakwaters are structurally more reliable since they have no moving parts or mooring requirements. Pile breakwaters also have the advantages such as easy pre-fabrication and small ecological footprint (by allowing water, marine life and sediment exchange across the breakwater). Thus, pile breakwaters are ideal for integrating with OWC devices for wave energy extraction and shore protection for sustainable coastal development.

The motivation of this study is to test a new wave-power plant concept shown in Fig. 1, which explores a new integration of OWC devices with a pile breakwater for wave energy extraction and shore protection. Traditional breakwaters such as caisson breakwaters or rubble mound breakwaters are expensive to build (on the order of 10 million Euros if they are built in shallow waters according to Sheehan and Harrington

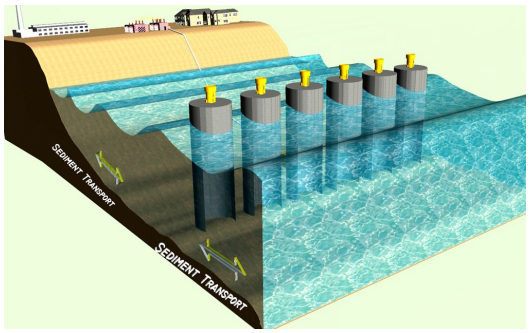

Fig. 1: An artistic view of the dual-functional wave-power plant for generation of wave-power electricity and shore protection. The yellow device on the top of each OWC-pile represents the power take-off device for generation of wave-power electricity. The design of the OWC pile is shown in Fig.2.

(2012)), which makes them unsuitable in places where water is relatively deep and the wave energy resource is rich. Pile breakwaters, however, can be constructed outside the surf zone with relatively low costs. The research described in this paper is built upon the theoretical and experimental work described in Deng et al. (2014) and Xu et al. (2016), where an OWC chamber is integrated into a single circular pile (referred to as an OWC-pile in this paper). The structure reported in this study is a dual-functional wave-power plant, which is in the form of a row of closely-spaced OWC-piles, for sustainable coastal development. Main results reported here include the characteristics of the nonlinear PTO-simulating device, the measured capture width ratio, reflection and transmission coefficients, and the estimated viscous dissipation due to vortex shedding from the OWC-piles. An evaluation of the performance of a scaled-up wave-power plant is also discussed.

2. OWC-pile wave-power plant model, experimental setup and test conditions

2.1. OWC-pile wave-power plant model

The left panel of Fig. 2 shows a small physical model of the proposed dual-functional wave-power plant. The model is a row of four identical closely-spaced OWC-piles. Each OWC-pile is an axisymmetric OWC device supported by a coaxial tube-sector-shaped structure (see the right panel of Fig.2), which has been studied theoretically by Deng et al. (2013) and experimentally by Xu et al. (2016).

Referring to the right panel of Fig. 2, the overall height of the OWC-pile was 40 cm, the outer diameter D was 12.5 cm, the thickness of the wall was 3 mm, the distance between the lower skirt of the chamber and the bottom of the wave flume D_s was 24.4 cm, and the opening angle of coaxial tube-sector-shaped structure was 180°. On the top of each OWC-pile, an orifice was used to simulate a power take-off (PTO) mechanism, and the diameter of the opening D_o was 1.4 cm, resulting in an opening-to-chamber ratio (the ratio of the area of the orifice to the inner cross-sectional area of

Fig. 2: Left: A row of four OWC-piles before its deployment in the wave flume. Right: a sketch of a single OWC-pile.

the OWC chamber) $\alpha = 0.0138$. In the experiment, each of the OWC-piles was made of stainless steel, and the lower skirt of the OWC chamber was carefully rounded using a rubber band to reduce possible energy loss associated with vortex shedding. Referring to the left panel of Fig. 2, four identical OWC-piles were closely mounted in a row onto a PVC plate of 3 mm in thickness to form a dual-functional OWC-pile wave-power plant model. The gap size between two adjacent OWC-piles D_g was 0.6 cm. The PVC top plate shown in the left panel of Fig. 2 ensured that all OWC-piles were upright and evenly spaced. After the model was placed in the wave flume, the bottom and top plates were firmly fixed with metal fixers on a structure attached to the wave flume, and the row of four OWC-piles was aligned to be perpendicular to the direction of wave incidence. To calculate the pneumatic power extraction, the air pressure and surface displacement in one of the OWC chambers (the second from the right in the left panel of Fig. 2) were measured using a pressure sensor and a wave gauge, respectively. See also the right panel of Fig. 2 for the locations of the pressure sensor and wave gauge.

In the determination of the gap size, one should consider the following key factors: wave transmission, water exchange across the structure, power-extraction efficiency. Based on previous theoretical studies of slotted/pile barrier breakwaters (e.g., Isaacson et al., 1998; Huang, 2007), a porosity of about 0.05 can provide an acceptable transmission coefficient for shore protection. For the OWC-pile diameter, a gap size of 0.6cm corresponds to a porosity of $n = 0.048$. The effects of the gap size on water exchange across the structure and power-extraction efficiency are worth further investigation, which is one of the topics of our future study for this project.

2.2. Experimental setup

A wave flume in the Hydraulic Modeling Laboratory at Nanyang Technological University was used for the experiment. The dimensions of the wave flume were 32.5-m long, 0.55-m wide and 0.6-m deep. At one end of the wave flume, a piston type wave maker was installed; at the other end of the wave flume, a 1:15 wave-absorbing

beach covered by porous material was installed to minimize wave reflection. The reflection coefficient of the wave-absorbing beach was less than 0.05 for wave periods ranging from 0.7 s to 1.6 s (He et al., 2013).

Referring to Fig. 3, the model was placed at 18.5 m from the wave maker. Two UltraLab ultrasonic sensors (S1 and S2) were installed at 7.5 m and 12.5 m from the wave maker, respectively; these two sensors were used to monitor the incident waves. In order to obtain the wave reflection coefficient using a two-point wave separation method (Goda and Suzuki, 1976), two resistance-type wave gauges, G4 and G5, were placed 15.7 cm apart in tandem, with gauge G5 being installed at 5 m from the model (i.e., 13.5 m from the wave maker). To determine the wave transmission through the dual-functional wave-power plant model and the beach reflection, two resistance-type wave gauges, G6 and G7, were placed 15.7 cm apart in tandem, with G6 being installed at 23.5 m from the wave maker. Wave gauge G2 was used to measure the surface displacement inside the OWC chamber, and wave gauges G1 and G3 were placed 30.5 cm in front of or behind the model to provide additional information for later numerical model validation. A piezo-electric type pressure sensor (P1) was mounted onto the top cover of the OWC chamber to measure the air pressure inside the OWC chamber. A camera (C1) was also installed on the front side of the flume to provide a side view of the waves interacting with the wave-power plant model. All sensors and camera were synchronized using a digital data acquisition device (DEWESoft DEWE-43), and the sampling rates of all devices were set to 50Hz.

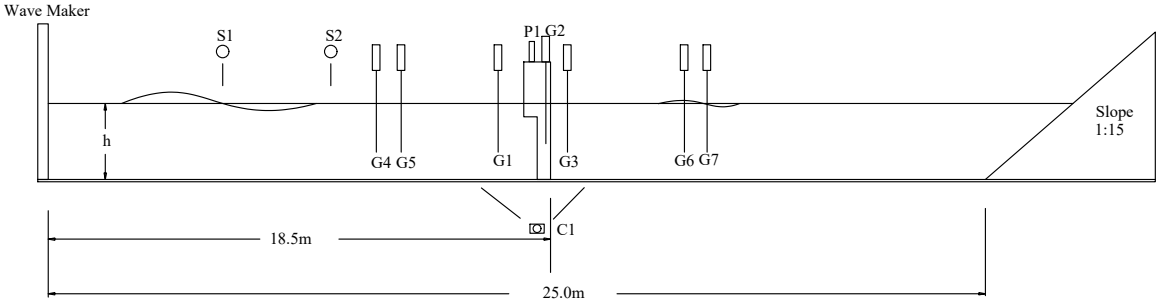

Fig. 3: Sketch of Experimental setup. Not drawn to scale.

2.3. Test conditions

The test conditions are summarized in Table 1. To test the effects of wave period and water depth on wave scattering and wave energy extraction, nine wave periods with a fixed wave height were tested for two water depths: $h = 0.29$ m (Case 1) and 0.31 m (Case 2). To test the effects of wave height on wave scattering and wave energy extraction, four wave heights, in combination with three wave periods were tested for a fixed water depth $h = 0.31$ m (Case 3). To evaluate the effects of the OWC chambers on wave reflection and transmission, which are important parameters for shore protection, the results from Cases 1-3 were compared with a set of existing tests

for a row of circular piles (without OWC chambers) of the same diameter and spacing in water depth of $h = 0.15$-0.3 m reported in Su (2013) (Cases 4-6); specifically, water depth was fixed at $h = 0.25$ m in Cases 4 and 5, and the wave height was fixed at H=0.029 m in Case 6. For all test conditions listed in Table 1, each test condition was repeated at least three times to minimize possible random error and ensure the repeatability of the test. The wave heights listed in the table are averaged values over three test runs, and the relative error in the measured wave heights for each test condition is less than 4%.

Table 1: Summary of test conditions, unit for period T is seconds, unit for water depth h and wave height H is cm.

With OWCs						Without OWCs					
Case 1		Case 2		Case 3		Case 4		Case 5		Case 6	
T	H	T	H	T	H	T	H	T	H	T	h
0.7	3.63	0.7	3.73	0.9	1.95	0.8	2.40	1.1	1.43	1.1	15
0.8	3.69	0.8	3.69	0.9	2.68	0.9	2.62	1.1	2.15	1.1	20
0.9	3.69	0.9	3.78	0.9	3.78	1.0	2.72	1.1	2.82	1.1	25
1.0	3.68	1.0	3.77	0.9	4.67	1.1	2.70	1.1	3.59	1.1	30
1.1	3.75	1.1	3.77	1.2	1.79	1.2	2.80	1.1	4.19	-	-
1.2	3.64	1.2	3.65	1.2	2.76	1.3	2.88	1.1	4.64	-	-
1.3	3.67	1.3	3.58	1.2	3.65	1.4	2.94	-	-	-	-
1.4	3.71	1.4	3.63	1.2	4.75	1.5	2.92	-	-	-	-
1.5	3.68	1.5	3.61	1.4	1.94	1.6	3.00	-	-	-	-
1.6	3.64	1.6	3.72	1.4	2.76	-	-	-	-	-	-
-	-	-	-	1.4	3.63	-	-	-	-	-	-
-	-	-	-	1.4	4.54	-	-	-	-	-	-

Typical piston-type wave makers for large wave flumes have a limitation on the shortest waves that can be generated, which is typically in the range of 0.7-1.0s. The test conditions must be chosen in consideration of the waves that the wave maker can generate and the resonant period of the OWC-pile model. For a single OWC-pile device identical to the individual OWC pile in the present dual-functional wave power plant model, the resonant period T_r is 0.617 s for $h/D = 2.32$ (0.694 s for $h/D = 2.48$) according to the quasi-linear theory of Xu et al. (2016). It is well known that the viscous effects may slightly increase the value of the resonant period obtained by potential flow theory. Therefore, the period of the shortest waves tested in the present experiment (T=0.7 s) should be very close to the actual resonant period of the standalone OWC-pile. Because the resonant period is mainly a property of the geometric configuration of an individual OWC pile, it is not expected to be affected by the presence of neighboring OWC piles.

3. Experimental data analysis

3.1. Determination of the characteristic coefficient of the quadratic PTO

Existing experimental studies of OWC devices usually use orifices to simulate their power take-off devices. Orifices in wave flume tests of OWC devices can simulate the velocity-pressure relationship, which is the key characteristics of PTO devices.

For small physical OWC models tested in wave flumes, the air can be treated as an incompressible fluid(He and Huang, 2017), and the pressure difference between the two sides of the orifice, Δp, can be expressed as

$$\Delta p(t) = \frac{1}{2} C_f \rho_a |u(t)| u(t) + \rho_a L_g \frac{du(t)}{dt}, \tag{1}$$

where $u(t)$ is the cross-sectional average velocity of the air inside the OWC chamber, ρ_a the density of air, C_f the quadratic loss coefficient, and L_g a length scale related to the inertia effect (Xu et al., 2016). The pressure-velocity model given in Eq.(1) is formally the same as the pressure-velocity relationship for water waves through a slotted barrier (Mei, 1989). For incompressible air, $u(t)$ is simply the cross-sectional average velocity of the water surface inside the OWC chamber.

In a previous experimental study of a single OWC-pile of identical dimensions, it has been shown that the inertia effect in Eq. (1) is not important (Xu et al., 2016). Therefore, the pressure-velocity relationship can be approximated by

$$\Delta p(t) = \frac{1}{2} C_f \rho_a |u(t)| u(t), \tag{2}$$

In the present experiment, the water surface inside the chamber was measured by a wave gauge at a single point, from which the vertical velocity at this point $u(t)$ was calculated; this wave gauge was located 3.7 cm behind the center point of the orifice (see the right panel of Fig.2). Appendix B shows that the error in the measured pneumatic efficiency caused by using one-point measurement to represent the cross-sectional average velocity is small for most of the test conditions examined in this study, except for several special periods.

3.2. Pneumatic power extraction and capture width ratio

The average pneumatic power extracted by one of the four OWC-piles within one wave period can be calculated by using the measured pressure $\Delta p(t)$ and the velocity $u(t)$

$$P_{OWC}^{(1)} = \frac{A_0}{T} \int_{t_0}^{t_0+T} \Delta p(t) u(t) dt, \tag{3}$$

where A_0 is the cross-sectional area of the pneumatic chamber, T is the wave period and t_0 is a reference instant of time. In view of Eq.(2), the average power extracted

by one OWC-pile in the wave-power plant model can be calculated by the measured pressure alone if the quadratic loss coefficient C_f is known,

$$P_{OWC}^{(1)} = \frac{A_0}{T} \int_{t_0}^{t_0+T} \sqrt{\frac{2|\Delta p(t)|^3}{C_f \rho_a}} dt, \tag{4}$$

Because the air pressure in the pneumatic chamber is approximately uniform except in a small region close to the orifice, one advantage of using Eq.(4) is that the calculated extraction of pneumatic power is not affected by: (i) the location of the pressure sensor as long as the sensor is installed in a location away from the orifice, and (ii) the non-uniformity of the water surface inside the OWC chamber.

A widely used concept in describing a WEC device is the so-called capture width (Martins-Rivas and Mei, 2009; Bingham et al., 2015; Xu et al., 2016), which is equal to the width of the wave crest of the incoming waves that contains the same amount of wave power being captured by the WEC device. For one of the OWC-piles in the wave-power plant model, the capture width λ is defined by

$$\lambda = \frac{P_{OWC}^{(1)}}{P_i} \tag{5}$$

where P_i is the mean incident wave power per unit crest width. Physically the average power extracted by an OWC device is equal to λP_i. According to linear wave theory, P_i is calculated by

$$P_i = \frac{1}{8} \rho_w g H^2 C_g, \tag{6}$$

where ρ_w is the density of water, g the gravitational acceleration, H the height of incident waves, and C_g the group velocity. The group velocity is calculated by linear wave theory as

$$C_g = \frac{1}{2} \left(1 + \frac{2kh}{\sinh(2kh)} \right) \frac{\omega}{k}, \tag{7}$$

where $\omega = 2\pi/T$ and $k = 2\pi/L$ with L being the wave length.

The capture width (λ) normalized by the diameter of OWC-pile (D), referred to as "capture width ratio", is a measure of the pneumatic power-extraction efficiency of an individual OWC-pile in the wave-power plant model. Therefore, the capture width ratio can be calculated by

$$\eta_{pneu} = \frac{\lambda}{D} = \frac{P_{OWC}^{(1)}}{P_i D}, \tag{8}$$

With the capture width ratio known, the power extracted by one of the OWC-piles in the wave-power plant model is

$$P_{OWC}^{(1)} = \eta_{pneu} D P_i \tag{9}$$

Therefore, the total pneumatic power that can be extracted by an OWC-pile wave-power plant consisting of N OWC-piles is

$$P_{OWC}^{(N)} = \eta_{pneu}(ND)P_i \tag{10}$$

The air compressibility is not important for small-scale models, but can be important for prototypes. If the model is scaled up by the Froude's law of similarity, the power-extraction efficiency for the prototype is slightly smaller than that for the model. The estimation of the power-extraction efficiency at full scale will be discussed later in Section 5.

3.3. Reflection and transmission coefficients

The sediment transport between the dual-functional wave-power plant and the shoreline is related to the waves transmitted through the power plant, while the waves reflected from the wave-power plant is related to the dynamic loading on the wave-power plant. To determine the wave reflection and transmission coefficients, four wave gauges (G4-G7) were installed at the locations shown in Fig.3. From the surface displacements measured by the wave gauges G4 and G5, the amplitudes of the incident (A_i) and reflected (A_r) waves were obtained through a two-point wave separation analysis; from the surface displacements measured by the wave gauges G6 and G7, the amplitudes of the transmitted waves (A_t) and the waves reflected from the wave-absorbing beach were obtained through a two-point wave separation analysis. The reflection (C_r) and transmission (C_t) coefficients are defined by

$$C_r = \frac{A_r}{A_i}, \quad C_t = \frac{A_t}{A_i} \tag{11}$$

Note that these two coefficients are defined for the fundamental frequency. Higher harmonic waves may exist in the vicinity of the OWC-pile breakwater due to the following reasons: (1) weakly nonlinear wave-wave interaction and (2) the radiated waves generated by the weakly nonlinear fluctuation of the air pressure inside the OWC chamber (see Section 3.1 for the quadratic nature of the air pressure). But in general, the higher harmonic waves are weak in our experiment.

4. Results

In this experimental study, the following parameters were fixed: the diameter of the OWC-piles (D), the distance between the lower tip of the skirt of the OWC chamber and the bottom (D_s), the diameter of the orifice (D_o), and the gap size between two adjacent OWC-piles (D_g). As shown in the dimensional analysis presented in Appendix A, all the results related to λ/D, C_r and C_t can be presented and discussed in terms of the following three dimensionless parameters: $T\sqrt{g/D}, H/D$ and h/D.

4.1. Characteristic coefficient of the quadratic PTO model

In this experimental study, the characteristic coefficient used to describe the behavior of the quadratic PTO model is the quadratic loss coefficient C_f defined by Eq.(2). The experimental results have shown that the parameter C_f is not sensitive to both H/D and $T\sqrt{g/D}$ and thus can be treated as a constant in the calculation of the capture width ratio.

Fig. 4 shows the fitted values of quadratic loss coefficient C_f for Cases 1 and 2, which were calculated using the velocity measured at one point inside the OWC chamber. It is remarked here that Cases 1 and 2 were designed to show how C_f would change with $T\sqrt{g/D}$. In Fig. 4, all values of C_f vary around a mean value $\bar{C}_f$ of 14,619 with a relative error less than $\pm 9\%$ (note that $\bar{C}_f$ was computed with results from both Fig. 4 and Fig. 5), except for $T\sqrt{g/D} = 6.20$ and 9.74 where the values of C_f are about 24% smaller than the mean — the values of C_f at these two wave periods were not included in the computation of the mean value of C_f due to large deviation. We attribute the deviation of C_f from the mean at $T\sqrt{g/D} = 6.20$ and 9.74 to the sloshing modes excited by higher harmonic waves and the one-point measurement method as explained in Appendix B.

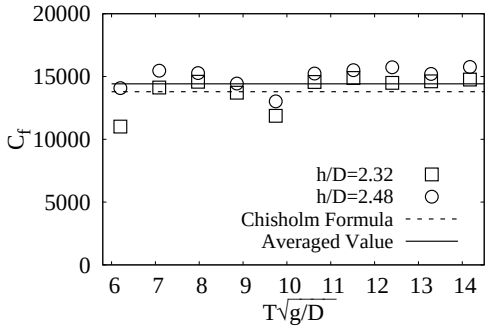

Fig. 4: Quadratic loss coefficient obtained using the one-point measured water surface elevation, results from cases 1 (squares) and 2 (circles) shown.

To show the change of C_f with the dimensionless wave height H/D, three wave periods ($T\sqrt{g/D} = 7.97, 10.63$ and 12.40) were selected and the dimensionless wave height H/D varied from about 0.144 to about 0.40 for each period. The change of C_f with H/D is shown in Fig. 5, from which it can be concluded that C_f is not sensitive to the variation of wave height in our experiment. It is remarked here that higher harmonic waves of these three periods cannot excite sloshing mode according to the analysis given in Appendix B.

In the following, an explanation to the behaviors of C_f shown in Figs. 4 and 5 is provided. The PTO is modeled by an orifice in this experimental study, and the key parameter to describe the flow through an orifice is the contraction coefficient C_c, which characterizes the ratio between the orifice area and the area at *vena contracta*. The quadratic loss coefficient of the orifice, C_f, can be determined by the following

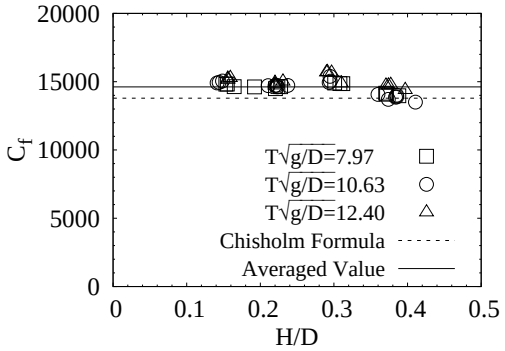

Fig. 5: Quadratic loss coefficient obtained using the one-point measured water surface elevation (Case 3).

expression for an oscillatory flow through an orifice,

$$C_f = (\frac{1}{\alpha C_c} - 1)^2. \tag{12}$$

where $\alpha = [D_o/D]^2$ is the opening ratio of the orifice (the reader is referred to Mei (1989) for a derivation of Eq.(12)). According to Eq. (12), the contraction coefficient corresponding to $\bar{C}_f$=14,619 in Figs. 4 and 5 is $C_c = 0.5945$. Previous experimental studies (Chisholm, 1983; Fossa and Guglielmini, 2002) have suggested the value of contraction coefficient can be determined by

$$C_c = \frac{1}{[0.639(1-\alpha)^{0.5} + 1]}. \tag{13}$$

For the present experiment, the opening ratio $\alpha = 1.38\%$, and Eq.(13) gives $C_c = 0.6118$, which corresponds to $C_f = 13,793$ according to Eq. (12).

For the results shown in Figs.4 and 5, the difference between the measured mean and the predicted values of C_f is 5.7%, which suggests that even though Eq.(13) is originally proposed for uni-directional flows, it nevertheless can provide a satisfactory prediction of the contraction coefficient C_c for oscillatory flow as well. This is consistent with the conclusions in our previous studies. Xu et al. (2016) tested a standalone OWC-pile of identical opening ratio in the same flume with identical wave conditions, and found that the fitted values of C_f fell within the range of 14,000 to 16,000 and were not sensitive to H/D and $T\sqrt{g/D}$. He and Huang (2017) performed a series of tests for circular orifices with the opening ratio ranging from 0.625% to 1.875%, and the contraction coefficient obtained using Eq. (12) fell within the range of 0.6109 to 0.6124, which are very close to the values predicted by Eq. (13), with a relative error being less than 1%.

The following conclusions can be drawn about the contraction coefficient C_c and the quadratic loss coefficient C_f from the results presented above:

(i) For an OWC chamber with a thin-wall circular orifice, the values of C_f and C_c are influenced mainly by the opening ratio and are not sensitive to both H/D and $T\sqrt{g/D}$ for small opening ratios under normal wave conditions.

(ii) The value of C_f is also not affected by the presence of other structures in the vicinity of the OWC chamber.

(iii) If the turbulent flows remain in the same regime, it is expected that Eq. (13) and Eq. (12) can be used to estimate the contraction coefficient C_c and quadratic loss coefficient C_f for thin-wall circular orifices with a relative error less than 6%.

In the following, the OWC pneumatic power is calculated using C_f=14,619.

4.2. Measured capture width ratio

The capture width ratio is an important parameter describing the wave energy extraction function of an OWC-pile dual-functional wave power plant. The variations of capture width ratio λ/D with $T\sqrt{g/D}$ for two values of h/D are shown in Fig.6, where the capture width ratio for a standalone OWC-pile tested in Xu et al. (2016) is also included for comparison. In general, the capture width ratio of an individual OWC-pile in the dual-functional wave power plant model is about 1.5-2.0 times larger than the capture width ratio of the corresponding standalone OWC-pile within the tested range of $T\sqrt{g/D}$, illustrating the significant influence of closely-spaced OWC-piles on the performance of individual OWC-piles in the dual-functional wave power plant model. The capture width ratio is not sensitive to small changes in water depth, except for the shorter waves tested in the experiment. Larger values of capture width ratio occur at smaller values of $T\sqrt{g/D}$ for all the cases shown in Fig. 6.

It is remarked that the maximum power output of a WEC device does not necessarily coincide with the maximum capture width ratio because the incident wave power changes with $T\sqrt{g/D}$. For real sea states, there is a joint distribution of wave height and period (Longuet-Higgins, 1983; Goda, 1999); therefore, the maximum capture width ratio cannot be obtained just from the variation of capture width ratio with frequency for a fixed height.

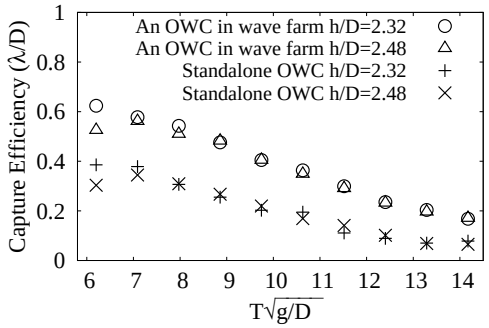

Fig. 6: Variations of capture width ratio with dimensionless wave period $T\sqrt{g/D}$ ($H/D = 0.296$).

The variations of capture width ratio λ/D with dimensionless wave height H/D are shown in Fig.7. The capture width ratio λ/D slightly increases with increasing H/D for $T\sqrt{g/D} = 10.63$ and 12.40, but the capture width ratio slightly decreases with H/D for $T\sqrt{g/D} = 7.97$. For practical purposes, the variation of capture width ratio with H/D is insignificant for $H/D > 0.2$.

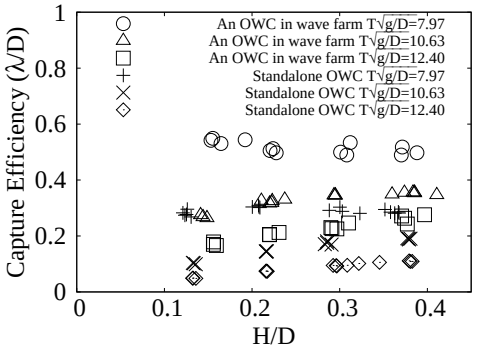

Fig. 7: Variations of capture width ratio with dimensionless wave height H/D ($h/D = 2.48$).

It is remarked here that the quasi-linear theory of Xu et al. (2016) has shown that the capture width ratio of a standalone OWC-pile device increases with increasing wave non-linearity (i.e., the wave height for a fixed wave period) until a threshold value, then begins to decrease with increasing wave non-linearity, which is in agreement with the numerical and experimental findings of López et al. (2015) and Wang et al. (2018). The same effect of wave non-linearity on capture width ratio is expected for a row of OWC-piles; however, due to the limitation of the highest waves that can be tested in the experiment, the peak capture width ratios are outside the tested range of H/D in Fig.7.

4.3. Wave reflection and transmission

In places where cross-shore sediment transport is responsible for beach erosion, it is desirable to reduce the wave energy reaching the shore. Therefore, wave transmission and reflection coefficients are two important hydrodynamic parameters describing the shore protection function of an OWC-pile dual-functional wave power plant. To understand possible effects of the power extraction by OWC chambers on the reflection coefficient (C_r) and the transmission coefficient (C_t), these two coefficients are compared for the OWC-pile dual-functional wave-power plant model and a row of closely-spaced piles of the same dimensions (i.e., the same pile diameter and the same gap size) under the same wave conditions.

4.3.1. Wave reflection and transmission for a row of closely-spaced piles

Su (2013) measured the reflection and transmission coefficients of a pile breakwater (a row of closely-spaced piles), which had a pile diameter and gap size identical to those used in the present study. The effects of H/D and $T\sqrt{g/D}$ on C_r and C_t for

one water depth ($h/D = 2.0$) and the effects of water depth h/D on C_r and C_t under a fixed wave height and period were studied in the experiment of Su (2013).

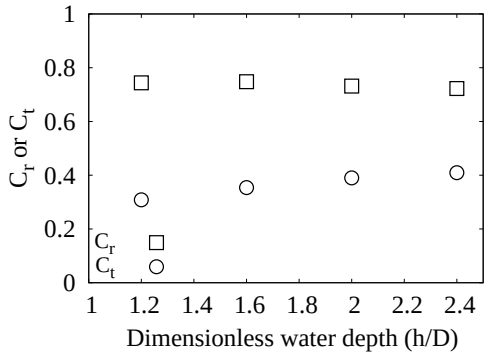

Fig. 8: Variation of reflection coefficient and transmission coefficient with dimensionless water depth h/D for the pile breakwater with $T\sqrt{g/D} = 9.74$ and $H/D = 0.228$.

Fig.8 shows the effects of dimensionless water depth h/D on C_r and C_t at $T\sqrt{g/D} = 9.74$ for the pile breakwater. Within the range of $h/D = 1.2$ to 2.4, the measured reflection coefficient C_r is not sensitive to changes in water depth, with a variation being less than 2%. The transmission coefficient C_t increases only slightly with the dimensionless water depth h/D; however, within the range of $h/D = 2.0$ to 2.4, the variation of C_t with h/D is less than 5%. For the two water depths examined in the present experimental study of the dual-functional wave power plant ($h/D = 2.32$ and $h/D = 2.48$), it has been shown in Section 4.2 that the capture width ratio is not sensitive to h/D in the tested range. It will be shown later in Section 4.3.2 that both the reflection and transmission coefficients obtained for these two water depths are almost the same for the dual-functional wave power plant model. Based on the information presented above, it can be concluded that by accepting a minimal amount of error within the range of $h/D = 2.0$ to $h/D = 2.48$, the effects of h/D on wave scattering can be ignored for both a pile breakwater (a row of closely-spaced piles) and an OWC-pile wave power plant model, and thus the effects of wave power extraction on C_r and C_t can be evaluated by comparing the reflection and transmission coefficients obtained from the following two experiments: (1) an OWC-pile wave-power plant model with $h/D = 2.32$ and $h/D = 2.48$, and (2) a row of closely-spaced piles of the same dimensions with $h/D = 2.0$.

4.3.2. Effects of power extraction on wave reflection and transmission

Variations of the measured reflection and transmission coefficients with dimensionless wave height H/D are shown in Fig. 9 for a fixed value of h/D=2.48 and three values of $T\sqrt{g/D}$. The results of Su (2013) for a row of closely-spaced piles of the same dimensions are also included in Fig. 9 for comparison. For a row of closely-spaced piles, because both C_r and C_t are not sensitive to h/D within the range of 2.0 to 2.4 (see Fig. 8), their values obtained for $h/D = 2.0$ are expected

to be close to those for $h/D = 2.48$. For the three values of $T\sqrt{g/D}$, the reflection coefficients for the OWC-pile wave power plant are significantly smaller than those for a row of closely-spaced piles of the same dimensions. While the reflection coefficient for a row of closely-spaced piles slightly decreases with H/D, the reflection coefficient of the OWC-pile wave power plant model is not very sensitive to H/D. The transmission coefficients for a row of closely-spaced piles are slightly larger than those for the OWC-pile wave power plant model. The transmission coefficients are slightly decreasing with H/D, regardless of the presence of the OWCs.

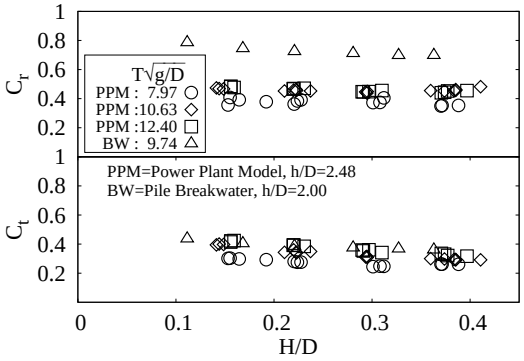

Fig. 9: Variations of C_r (top panel) and C_t (bottom panel) with dimensionless wave height H/D for various dimensionless wave period $T\sqrt{g/D}$.

Variations of the measured reflection and transmission coefficients with $T\sqrt{g/D}$ are shown in Fig. 10 for two values of h/D; the results for a row of closely-spaced piles of the same dimensions, studied by Su (2013), are also included in Fig. 10 for comparison. Within the tested range of h/D, the transmission coefficient increases with $T\sqrt{g/D}$ for a fixed wave height, regardless of the presence of the OWCs. It is interesting to note that the power extraction by the nonlinear PTO only slightly reduces the transmission coefficient. The reflection coefficient for a row of closely-spaced piles decreased noticeably with $T\sqrt{g/D}$, but the reflection coefficient for the OWC-pile wave power plant model is not very sensitive to $T\sqrt{g/D}$. As far as shore protection is concerned, integrating OWCs into a pile breakwater can not only achieve the same degree of shore protection as a pile breakwater does, but also effectively reduce the reflected waves (i.e., the wave loading on the structure), which can improve the structural reliability and reduce construction costs.

An intuitive explanation is provided here to help understand the results presented in Figs.6 and 10. Wave energy extraction is directly related to the up-and-down motion of the water surface inside the OWC chamber: for a given chamber-PTO design, a larger up-and-down motion for a given wave period always results in a larger fluctuation of the air pressure inside the OWC pneumatic chamber, and thus more energy being extracted by the PTO [see Eq. (4)].

In the absence of OWC chambers, wave reflection is caused mainly by the outer surface of the piles, resulting in a partial standing wave and thus an enhanced up-

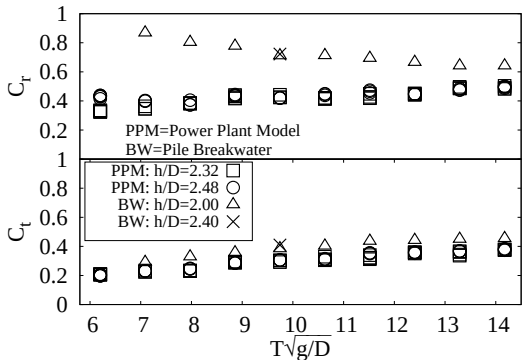

Fig. 10: Variations of C_r (top panel) and C_t (bottom panel) with dimensionless wave period $T\sqrt{g/D}$ for different dimensionless water depth h/D.

and-down motion of the water surface in front of the breakwater. Experimental and theoretical results (i.e., Kakuno and Liu, 1993) have shown that a shorter wave tends to have stronger wave reflection (i.e., a larger up-and-down motion in front of the breakwater). When OWC chambers are integrated into the pile breakwater, wave reflection is caused by the outer surface of the OWC chamber, the back wall of the OWC chamber, and the support structure underneath the OWC chamber. In addition to wave reflection, the fluctuation of the air pressure inside the OWC chamber also generates radiated waves, which can affect the wave field in front of the OWC-piles as well. The wave reflection caused by the back wall of the OWC chamber and the support structure enhances the up-and-down motion inside the OWC chamber, which is stronger for shorter waves. The up-and-down motion inside the OWC chamber is responsible for the wave-power extraction by the PTO and the generation of the radiated waves. Because only a portion of the energy associated with the radiated waves and the waves reflected by the back wall of the OWC chamber and the support structure can propagate out of the OWC chamber, the reflected waves for the OWC-piles are not as strong as those for a pile breakwater of the same dimensions. The support structure and the small gap make it difficult for the radiated waves to propagate to the lee side of the OWC-piles, and it is the ratio of the gap size to the diameter of the pile (the porosity of the structure) that largely controls the transmitted waves. This explains (i) why larger capture width ratio occurs towards the end of shorter waves (see Fig. 6), (ii) why integrating OWCs into a pile breakwater can reduce both the reflection and transmission coefficients, and (iii) why the power extraction has more significant effect on the reflection coefficients of shorter waves but less effect on the transmission coefficients.

4.4. Wave power removal from wave field and viscous dissipation

For the OWC-pile dual-functional wave power plants, in addition to the energy dissipated into the unusable energy of turbulence through vortex shedding, a portion of the wave power is removed from the wave field by the PTO to generate electricity.

Therefore, it is important to know how much wave power is unusable for the OWC-pile dual-functional wave power plants to generate electricity.

It is remarked that both the energy dissipated into turbulence and the energy extracted by the PTO are removed from the wave field. For a row of closely-spaced piles, wave power is removed from the wave field only through viscous dissipation associated with the vortex shedding from the piles, and a dissipation coefficient is often used in the literature to quantify the wave power dissipated into the unusable energy of turbulence. Next, the conservation of wave power is examined to quantify the energy dissipated by vortex shedding and the wave power extracted by the PTO.

Assuming that a row of N OWC-piles fits the width of the wave flume B, the conservation of wave power requires that

$$P_iB = \underbrace{C_r^2 P_iB + C_t^2 P_iB}_{(i)} + \underbrace{N\eta_{pneu} D P_i}_{(ii)} + \underbrace{C_d^{(vis)} P_iB}_{(iii)} \tag{14}$$

where the left hand side is the incident wave power, the term (i) is the wave power in the reflected and transmitted waves, term (ii) is the wave power extracted by the PTO, and term (iii) is associated with the energy dissipated into turbulence. The coefficient $C_d^{(vis)}$ is the so-called viscous dissipation coefficient. It is remarked here that in steady state (i.e., in regular waves after the ramping-up process), the amount of the energy associated with the heave motion of the water column inside an OWC chamber does not change with time; therefore it should not be included in the conservation of wave power as a sink or source term.

Eq. (14) can be rewritten as

$$1 = C_t^2 + C_r^2 + C_d^{(OWC)} + C_d^{(vis)} \tag{15}$$

where $C_d^{(OWC)}$ is the power extraction coefficient of the dual-functional wave-power plant and defined by $C_d^{(OWC)} = (1-\epsilon)\eta_{pneu}$ with $\epsilon = (B - ND)/B \ll 1$ being the porosity of the row of OWC-piles. Because $\epsilon \ll 1$ in the dual-functional wave power plant, $C_d^{(OWC)} \approx \eta_{pneu}$, which is independent of the number of OWC-piles used in the power plant. Therefore, it is possible to use Eq. (15) to provide an estimate of the viscous dissipation coefficient $C_d^{(vis)}$ from the measured values of C_t, C_r and η_{pneu}. For later discussion, a wave-power removal coefficient C_d is introduced, which is defined by

$$C_d = C_d^{(OWC)} + C_d^{(vis)} \tag{16}$$

Note that for a row of closely-spaced piles without OWCs, $C_d = C_d^{(vis)}$.

The top panel in Fig. 11 shows the variation of wave-power removal coefficient C_d with dimensionless wave height H/D, and the bottom panel in Fig. 11 shows the variation of the wave-power removal coefficient C_d with dimensionless wave period $T\sqrt{g/D}$. The wave-power removal coefficients C_d for a row of piles without OWCs are also included in Fig. 11 for comparison.

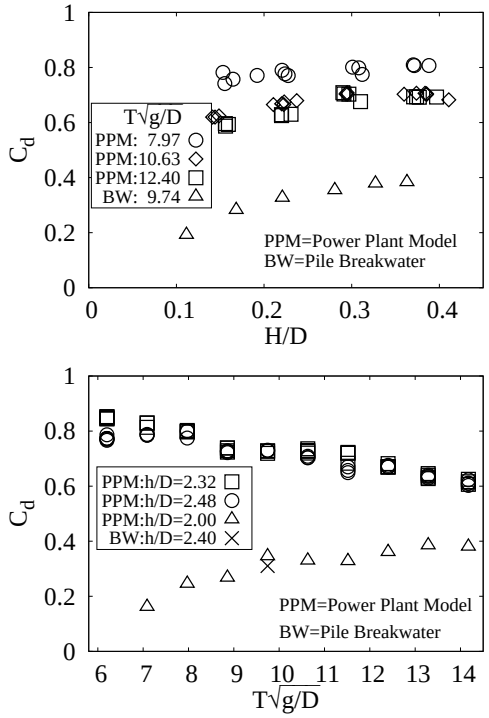

Fig. 11: Variations of wave-power removal coefficient C_d with dimensionless wave height H/D (top panel) and dimensionless wave period $T\sqrt{g/D}$ (bottom panel).

For the pile breakwater studied by Su (2013), the wave-power removal coefficient $C_d = C_d^{(vis)}$, which is simply the traditional dissipation coefficient. It can be seen from Fig. 11 that C_d increases with increasing either H/D or $T\sqrt{g/D}$ when other parameters are fixed. The amount of wave power removed from the wave field by the pile breakwater (i.e., the viscous dissipation coefficient $C_d^{(vis)}$) increases from about 20% of the incident wave power for $T\sqrt{g/D}$=7.08 to about 40% for $T\sqrt{g/D}$=14.17. However, the amount of wave power removed from the wave field by the dual-functional wave-power plant model, which includes both viscous dissipation and wave power extraction by the PTO, is significantly larger than that for the pile breakwater for any given wave period, reaching 80% of the incident wave power for short waves. Note that the value of C_d is only weakly sensitive to the variation in wave height, but decreases with increasing wave period.

The wave-power removal coefficient $C_d = C_d^{(OWC)} + C_d^{(vis)}$ can be calculated from the measured wave reflection and transmission coefficients using Eq. (15); the wave power extraction coefficient $C_d^{(OWC)}$ can be calculated from the measured air pressure and the surface displacement in the OWC chamber using Eqs. (4) and (8); as a result, the viscous dissipation coefficient $C_d^{(vis)}$ for the dual-functional wave power plant can be calculated and compared with that for the pile breakwater.

In the following, a semi-theoretical model is presented to understand the behaviors of $C_d^{(vis)}$ for an OWC-pile dual-functional wave power plant model and a pile

breakwater of the same dimensions. In particular, the semi-theoretical model will show that $C_d^{(vis)}$ increases with wave steepness kH (k is the wave number and H the wave height) and the third power of transmission coefficient (i.e., C_t^3), which causes C_d for the pile breakwater to increase with $T\sqrt{g/D}$ within the tested range.

4.5. A semi-theoretical model for viscous dissipation

Since the work done by the wave force acting on the piles is directly related to the wave power dissipated into turbulence, a semi-theoretical model can be devised to help understand the change of $C_d^{(vis)}$ with H/D, D/h and $T\sqrt{g/D}$.

The semi-theoretical model presented here is based on the work done by the wave force acting on a single pile, denoted by $W^{(1)}$. The wave force acting on a segment of a pile /OWC-pile of length dz can be estimated by the following Morison equation (Mei, 1989)

$$dF = \frac{1}{2}\rho_w C_D D|u|udz + \rho_w C_M \frac{\pi D^2}{4}\frac{du}{dt}dz \tag{17}$$

where u is the local horizontal orbital velocity immediate downstream of the pile/OWC-pile, C_D and C_M are empirical drag and inertia coefficients, respectively. It is remarked that the values of C_D and C_M for piles may be different from those for OWC-piles. For one pile/OWC-pile, the net work done by the inertia force over one wave period is zero; therefore, the net work done by the wave force dF over one wave period is

$$dW^{(1)} = T\left(\overline{dF \times u}\right) \equiv \frac{C_D T}{2}\rho_w D\overline{|u|^3}dz \tag{18}$$

where the over-bar means taking a time average over one wave period. It then follows that the net work done by the drag force acting on a pile/OWC-pile over one wave period is

$$W^{(1)} = T\int_{-h}^{0}\frac{C_D}{2}\rho_w D\overline{|u|^3}dz \tag{19}$$

As a first estimate, the empirical drag coefficient C_D is assumed to be a constant for the values of Reynolds number (Re) and Keulegan-Carpenter number (KC) used in the model tests. The constant drag coefficient C_D is treated as a fitting parameter in this semi-theoretical model.

The total wave power dissipated by a row of N closely-spaced piles/OWC-piles over one wave period is

$$W^{(N)} = NW^{(1)} \tag{20}$$

According to the conservation of wave power, $W^{(N)}$ should be equal to $TC_d^{(vis)}P_iB$ with B being the width of the row. It then follows that

$$C_d^{(vis)} = \rho_w \frac{C_D}{2P_i}\frac{ND}{B}\int_{-h}^{0}\overline{|u|^3}dz \approx \rho_w \frac{C_D}{2P_i}\int_{-h}^{0}\overline{|u|^3}dz \tag{21}$$

where $B \sim (ND)$ has been used in the last equation for closely-spaced piles/OWC-piles. For linear waves, the downstream velocity u can be expressed in terms of the transmission coefficient C_t as

$$u = \frac{\omega H C_t}{2} \frac{\cosh(k(h+z)}{\sinh(kh)} \sin(\omega t), \tag{22}$$

and the wave power P_i is

$$P_i = \frac{1}{8}\rho_w g H^2 C_g,\ C_g = \frac{1}{2}\left(1 + \frac{2kh}{\sinh(2kh)}\right)\frac{\omega}{k}. \tag{23}$$

It then follows that

$$C_d^{(vis)} \approx \frac{4 C_D C_t^3 kH}{3} N(kh) \tag{24}$$

where the function $N(kh)$ is given by

$$N(kh) = \frac{[\sinh(3kh) + 9\sinh(kh)]\tanh(kh)}{12\sinh^2(kh)[\sinh(kh) + 2kh]} \tag{25}$$

Note that kH can be written in terms of kh, H/D and D/h as

$$kH = (kh)\left(\frac{H}{D}\right)\left(\frac{D}{h}\right) \tag{26}$$

The linear wave dispersion

$$\frac{\omega^2 h}{g} = kh \tanh kh, \tag{27}$$

can be rewritten as

$$\left(T\sqrt{g/D}\right)\left(\sqrt{D/h}\right) = \frac{2\pi}{\sqrt{kh\tanh(kh)}} \tag{28}$$

From Eq. (28) the dimensionless parameter kh is an implicit function of D/h and $T\sqrt{g/D}$, and from Eqs. (26) and (28) the dimensionless parameter kH is an implicit function of D/h, H/D and $T\sqrt{g/D}$. Therefore, the viscous dissipation coefficient $C_d^{(vis)}$ given in Eq. (24) is a function of H/D, D/h, $T\sqrt{g/D}$, C_D and C_t.

For a circular cylinder in waves, it has been known that the drag coefficient C_D is a function of the Keulegan-Carpenter number ($KC = C_t \pi H/D$) and Reynolds number (Re). For a pile/OWC-pile, the Reynolds number can be defined by

$$Re = \frac{C_t \omega (H/2) D}{\nu} \tag{29}$$

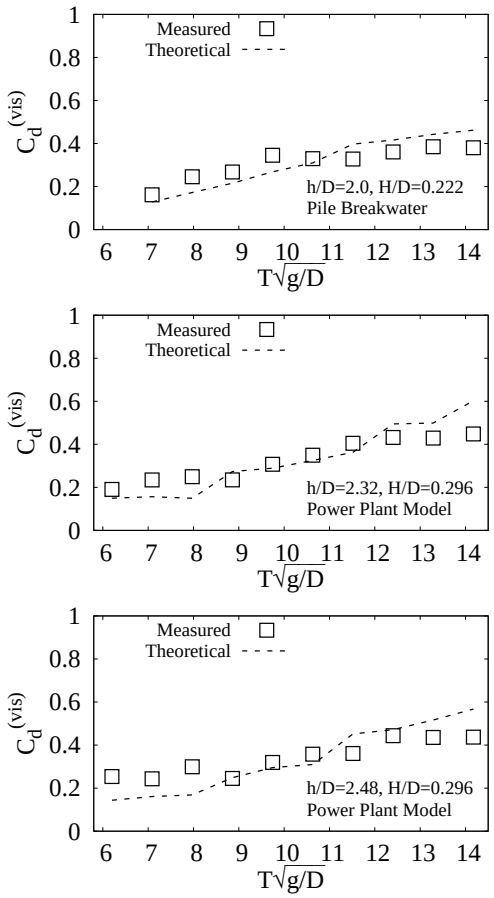

Fig. 12: Changes of predicted and measured viscous dissipation coefficients with dimensionless period for the pile breakwater model (top panel) and the dual-functional wave power plant model (middle and bottom panels).

According to the DNV guideline (DNV-GL, 2007), C_D can be written as

$$C_D = C_D^0 \psi(KC) \tag{30}$$

where C_D^0 is the drag coefficient for steady flow and $\psi(KC)$ is a wave amplification factor. For the tested range of Reynolds number (1604.7 to 2213.8) and KC number (0.15 to 0.360), the value of C_D^0 can be treated as a constant and the value of $\psi(KC)$ have a variation of less than 25% (please refer to Item 6.7 of DNV-GL (2007) for details). Therefore, it is reasonable to assume a constant C_D in all tested conditions for the purpose of providing a rough estimation of the variation of the viscous dissipation coefficient $C_d^{(vis)}$.

Using the measured transmission coefficients C_t corresponding to the given values of H/D, D/h and $T\sqrt{g/D}$, a non-linear least square data fitting of Eq. (24) to the measured $C_d^{(vis)}$ can be performed to determine a constant value of C_D. The predicted and measured viscous dissipation coefficients for the pile breakwater model and the

dual-functional wave-power plant model are shown in Fig. 12 for Cases 1, 2 and 4, and in Fig. 13 for Cases 3 and 5. For the pile breakwater model, the fitted value of C_D is 107.2; for the OWC-pile dual-functional wave power plant model, the fitted value of C_D is 216.6. As expected, the drag coefficient C_D for the OWC-pile is larger than that for a circular pile whose shape is more streamlined.

It can be seen from Figs. 12 and 13 that the semi-theoretical model can capture the variations of $C_d^{(vis)}$ with $T\sqrt{g/D}$ and D/h reasonably well. Because the transmission coefficients C_t used in producing Figs. 12 and 13 are measured ones, which contain random errors, the predicted curves for $C_d^{(vis)}$ are not smooth. The values of viscous dissipation coefficients $C_d^{(vis)}$ are similar for both structures (an OWC-pile dual functional wave power plant model and a pile breakwater model of the same dimensions). For both structures, $C_d^{(vis)}$ increases with increasing $T\sqrt{g/D}$ for given values of D/h and H/D. For the pile breakwater model $C_d^{(vis)}$ increases with increasing H/D for given values of D/h and $T\sqrt{g/D}$; for the dual-functional wave-power plant model, $C_d^{(vis)}$ appears to be less sensitive to H/D.

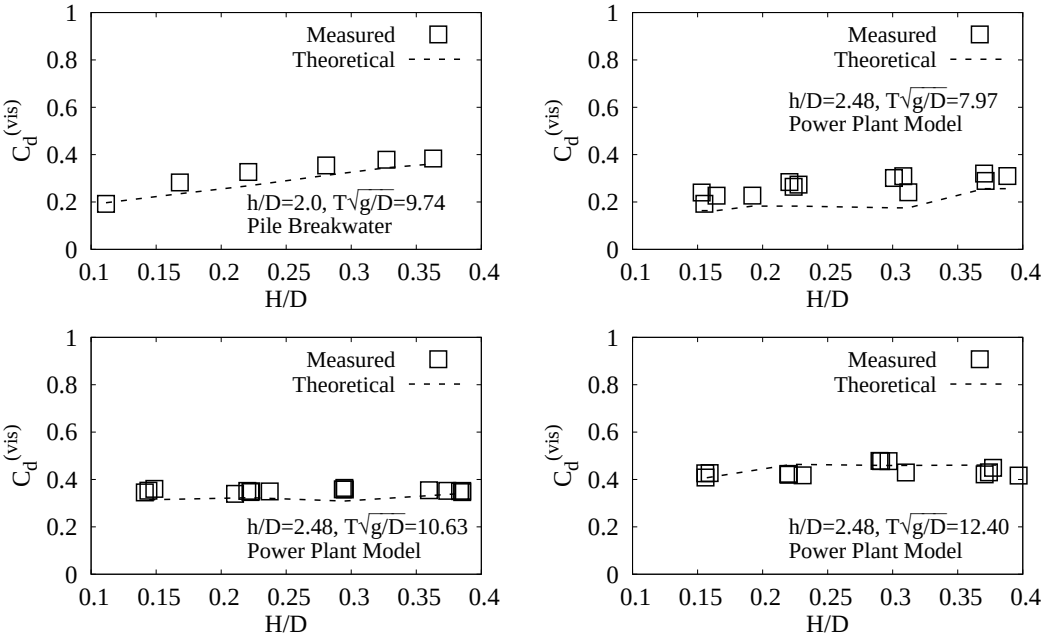

Fig. 13: Changes of predicted and measured viscous dissipation coefficients with dimensionless wave height for the pile breakwater model (top left panel) and the dual-functional power plant model.

It is remarked that the dual-functional wave-power plant model and the pile breakwater model of the same dimensions have similar values of viscous dissipation coefficient. As a result, the semi-theoretical model also predicts a larger drag coefficient for the dual-functional wave power plant model because the transmission coefficient of the dual-functional wave power plant model is about 20% smaller than that of the pile breakwater model of the same dimensions. Numerical simulations are needed to

further understand the increase of drag coefficient C_D caused by integrating OWC chambers into a pile breakwater. Three-dimensional numerical simulations of the OWC-pile dual functional wave-power plants is computationally challenging if the PTO is explicitly modeled. This is due mainly to the challenge posed by modeling the thin walls and the high velocity of the air flow through the PTO, which requires very fine grid size and very small time steps in order to satisfy the CFL stability condition. The small time step and the large number of cells created by a three-dimensional mesh require the simulation be run on a high performance computing facility.

5. A full-scale dual-functional wave-power plant

For a full-scale dual-functional wave-power plant designed according to Froude's law of similarity, the Keulegan-Carpenter number is invariant and the Reynolds number is scaled by $s^{3/2}$ where s is the geometric scale factor. If the diameter of the full-scale OWC-pile is 3.13 m, the geometric scale factor is $s = 25$ based on the model tested in this study. From the range of Re in the model test, one can obtain $Re = 1.9 \times 10^5 - 2.6 \times 10^5$ at the full scale. It is expected that the drag coefficient C_D used in Eq. (24) for estimating the viscous dissipation coefficient is not very sensitive to Reynolds numbers because C_D^0 is not sensitive to Reynolds number in the range of $O(10^3)$ to $O(10^5)$. It is, therefore, reasonable to assume that the viscous dissipation coefficient $C_d^{(vis)}$ presented in Fig. 12 is approximately valid at the full scale, which will allow us to evaluate the performance of a dual-functional wave-power plant at full scale.

The electric power output of a single OWC device is affected by its pneumatic efficiency, η_{pneu}, the rotor efficiency η_{rtr}, and the efficiency of electric generator η_{gen}. For typical impulse turbines, η_{rtr} can be as large as 0.5 (Setoguchi et al., 2001). A recent study (Falcão et al., 2013) shows that η_{rtr} for self-rectifying radial-flow air turbines can be as large as 0.7. Modern electric generators are very efficient, and can achieve $\eta_{gen} \sim 1$.

For any OWC-pile in a dual-functional wave-power plant consisting of N OWC-piles, the electric power output of this OWC-pile is related to the pneumatic power $P_{OWC}^{(1)}$ by

$$P^{(1)} = \eta_{gen} \underbrace{\left[\eta_{rtr}\, \eta_{air}\, P_{OWC}^{(1)}\right]}_{\text{shaft power output}}. \tag{31}$$

where η_{air} is a compressibility-effect coefficient representing the effects of air compressibility on the pneumatic power efficiency. According to Elhanafi et al. (2016b), $\eta_{air} \sim 1$ for small scale models and $\eta_{air} \sim 0.88$ for prototype models. After using the expression for $P_{OWC}^{(1)}$ given in Eq. (9), the following expression is obtained

$$P^{(1)} = \eta_{gen}\, \eta_{rtr}\, \eta_{air}\, \eta_{pneu} DP_i. \tag{32}$$

Therefore, the total electric power output of a dual-functional wave-power plant consisting of N OWC-piles can be estimated by

$$P^{(N)} = \eta_{gen}\,\eta_{rtr}\,\eta_{air}\,\eta_{pneu}(ND)P_i. \tag{33}$$

Eq.(33) is to be used to estimate the electric power output of a dual-functional wave-power plant at full scale. the following values are used in the calculation: the OWC pneumatic efficiency η_{pneu} from respective scaled-down wave periods in Fig.6, the rotor efficiency $\eta_{rtr} = 0.7$ for the turbine (Falcão et al., 2013), the generator efficiency of $\eta_{gen} = 0.9$. The dual-functional wave power plant is to be designed according to $D = 3.13$ m and $h/D = 2.40$, which corresponds to a geometric scale of about 25 and a water depth of 7.25 m to 7.75 m. The compressibility-effect coefficient $\eta_{air} = 0.88$ is used to reflect the effects of air compressibility on the pneumatic power efficiency at full scale.

The dual-functional wave-power plant is deployed along a 1000-m straight coastline. The electric power outputs for six wave conditions are listed in Table 2; these six wave conditions reflect the seasonal change of wave climate as well as the tidal change at the site. Mean wave period T and root-mean-square wave height H are used to estimate the wave power P_i. Scenario 1 and 2 correspond to the test conditions with T=1.1 s of Cases 1 and 2, respectively, in Table 1; Scenario 3 and 4 correspond to the test conditions with T=0.8 s of Cases 1 and 2, respectively, in Table 1; Scenario 5 corresponds to the test condition with T=0.9 s and H=0.0467 m of Case 3 in Table 1; Scenario 6 corresponds to the test condition with T=1.4 s and H=0.0454 m of Case 3 in Table 1. The water depth for Scenarios 1 and 3 is 7.25 m, and the water depth for Scenarios 2, 4, 5 and 6 is 7.75 m, reflecting a tidal range of 0.5 m at the project site.

A comparison of the electric power outputs between Scenarios 1 and 2 and between Scenarios 3 and 4 shows that a tidal range of 0.5 m does not significantly change the electric power output, which varies from 1.0 Mw to 1.2 Mw for the typical coastal waves with periods in the range of 4.0 s and 5.5 s and wave heights in the range of 0.92 m and 0.94 m; these wave conditions are representative of mild wave conditions near shore. Compared to the pile breakwater with the same dimensions, the OWCs help reduce the reflection coefficients from 0.72 to about 0.43 for Scenarios 1 and 2, and from about 0.87 to less than 0.40 for Scenarios 3 and 4. Therefore, the dual-functional wave power plant can generate about 1.0 Mw electricity and achieve a better shore protection than a traditional pile breakwater under typical near-shore wave conditions.

Scenarios 5 and 6 represent two cases of slightly larger wave height corresponding to mild extreme wave events. Comparing Scenario 5 and Scenario 4, an about 27% increase in wave height and an about 12.4% increase in wave period result in an about 70% increase in the electric power output and an almost unchanged transmission coefficient. Comparing Scenarios 5 and 6, increasing wave period form 5.5 s to 7.0 s slightly reduces the electric power output and increases the transmission coefficient

from 0.26 to 0.36, which is still significantly smaller than the value of 0.67 for the transitional pile breakwater.

Table 2: Electric power output estimates for the hypothetical power plant

Scenario	T [s]	h [m]	H [m]	C_r	C_t	P_i [kW]	$T/\sqrt{g/D}$	H/D	η_{pneu}	Power [MW]
1	5.5	7.25	0.94	0.43	0.30	5.57	9.74	0.300	0.41	1.21
2	5.5	7.75	0.94	0.42	0.31	5.60	9.74	0.301	0.41	1.22
3	4	7.25	0.92	0.35	0.23	3.64	7.08	0.294	0.58	1.12
4	4	7.75	0.92	0.40	0.23	3.58	7.08	0.294	0.56	1.07
5	4.5	7.75	1.17	0.35	0.26	6.80	7.97	0.374	0.50	1.81
6	7	7.75	1.14	0.45	0.36	10.02	12.39	0.364	0.27	1.44

It can be concluded from Table 2 that (i) the power output of about 1.0-1.8 MW can be achieved under seasonal changes of wave conditions and the influence of a 0.5-m tidal range, and (ii) integrating the OWC into the pile breakwater can significantly improve the pile breakwater's performance in reducing wave transmission and thus cross-shore sediment movement between the wave-power plant and the shoreline. The electric power output of this dual-functional wave-power plant is roughly equivalent to three wind turbines with a rotor diameter of 40 m under typical wind speeds suitable for wind turbines. However, the main advantages of the dual-functional wave-power plant include: (i) low construction costs by sharing the construction cost with breakwaters and (ii) shore-protection functionality. Because the costs of wave-power plant increase sharply with increasing requirements on structural strength and safety, it is desirable, from an economical point of view, to have wave-power plant designed for mild wave conditions but can still survive extreme wave conditions, which is exactly the design principle for pile breakwaters. The significant reduction of the reflection coefficient by integrating the OWCs into the pile breakwater can also increase the survivability of the dual-functional wave power plant.

The OWC-pile type of dual-functional wave-power plants is recommended for places where pile breakwaters are to be built for shore protection; the additional costs (other than the necessary equipment related to PTO and Power Grid connection) to integrate the OWC chambers into the pile breakwater may not be a concern due to the simplicity of the OWC-pile structure. Integrating OWC chambers into the pile breakwater may improve the survivability of structure through reduction of the reflection coefficient (see Fig. 10); however, the structural strength aspect of the OWC-pile power plant still needs to be evaluated separately. The findings of the present research promote close collaboration between wave-energy utilization community and the shore-protection community for commercial-scale deployment of WECs and contribute to making wave energy economically competitive.

6. Conclusions

In this study, the performance of a dual-functional wave-power plant based on the concept of integrating oscillating water columne (OWC) chambers into a pile breakwater is evaluated through a series of wave flume tests. The OWC-pile wave-power plant can serve as a breakwater for shore protection for sustainable coastal development, which provides a viable way to achieve cost sharing between two functions of the structure and to improve the structure's survivability. Our experimental results have shown that integrating OWC chambers into a pile breakwater can significantly increase the capture width ratio of the OWC chambers as compared with standalone OWC-piles, making it possible to design the OWC-pile type of dual-functional wave-power plants to operate under mild wave conditions. Integrating OWC chamber into the pile breakwater can also reduce both the reflection coefficient and transmission coefficients; this additional reduction in wave reflection and transmission can improve shore-protection performance and reduce the wave loading on the structure and improve the survivability of the structure. The additional reduction of transmission coefficient is introduced mainly by the wave-power extraction of the power take-off device. The viscous dissipation due to vortex shedding from the piles is less influenced by the integration of OWCs. A dual-functional wave-power plant at a full scale proposed for a 1000 m-long coastline with typical mild coastal wave conditions can provide an electric power output of about 1.0 to 1.8 MW and much lower wave transmission under typical seasonal wave conditions and the influence of a 0.5-m tidal range. The findings of this work promote close collaboration between wave-energy utilization community and the shore-protection community for commercial-scale deployment of wave energy converters and contribute to making wave energy economically competitive.

7. Acknowledgments

The material is based on work supported by the National Science Foundation under grant No. CBET-1706938. Any opinions, findings, and conclusions or recommendations expressed in this material are those of the author(s) and do not necessarily reflect the views of the National Science Foundation. This is SOEST contribution No. 10428.

Appendix A. Dimensional analysis

For the model examined in this study, the capture width ratio λ/D [defined by Eq.(8)], the reflection coefficient C_r and the transmission coefficient C_t of the OWC-pile breakwater can be expressed in functional forms as

$$(\lambda/D, C_r, C_t) = f(h, H, T, D, D_t, D_g, D_r, D_o, \rho_w, \rho_a, g, \nu_w, \nu_a), \tag{A.1}$$

where h is the water depth, H the incident wave height, T the wave period, D the outer diameter of the OWC-pile, D_g the gap between two adjacent OWC-piles, D_r

is the draft of the OWC chamber, D_o is the opening diameter of the orifice, and D_t is the thickness of the skirt of the OWC chamber. The distance between the tip of the OWC skirt and the bottom is $D_s = h - D_r$. The physical constants g, ρ_w, ρ_a, ν_w, and ν_a are the gravitational acceleration, the density of the water, the density of the air, the kinematic viscosity of the water, and the kinematic viscosity of the air, respectively.

Using Buckingham π -theorem, Eq. (A.1) can be reduced to the following dimensionless form

$$\left(\frac{\lambda}{D}, C_r, C_t\right) = f\left(\frac{gT^2}{D}, \frac{h}{D}, \frac{H}{D}, \frac{\rho_w}{\rho_a}, \frac{\nu_a T}{D^2}, \frac{\nu_w T}{D^2}, \frac{D_t}{D}, \frac{D_g}{D}, \frac{D_s}{D}, \frac{D_o}{D}\right). \tag{A.2}$$

Combining H/D with $\nu_w T/D^2$ (or $\nu_a T/D^2$) gives $\nu_w T/(DH)$ (or $\nu_a T/(DH)$), which can be written as ν_w/DU (or ν_a/DU), respectively, with $U = H/T$ being a velocity scale. Combining D_o/D with ν_a/DU gives $\nu_a/D_o U$. Therefore, Eq. (A.2) can be further written as

$$\left(\frac{\lambda}{D}, C_r, C_t\right) = f\left(T\sqrt{\frac{g}{D}}, \frac{h}{D}, \frac{H}{D}, \frac{D_t U}{\nu_w}, \frac{D_o U}{\nu_a}, \frac{DU}{\nu_w}, \frac{D_t}{D}, \frac{D_s}{D}, \frac{D_g}{D}, \frac{D_o}{D}\right). \tag{A.3}$$

In this experiment,the last four parameters are constant. In this study, both ν_w and ν_a are fixed: if $T\sqrt{g/D}$ and h/D are fixed, then $D_t U/\nu_w, DU/\nu_w$ and $D_o U/\nu_a$ will be functions of H/D; if H/D and h/D are fixed, then $D_t U/\nu_w, DU/\nu_w$ and $D_o U/\nu_a$ will be functions of $T\sqrt{g/D}$. Therefore, all the results related to λ/D, C_r and C_t can be presented and discussed in terms of $T\sqrt{g/D}, H/D$ and h/D in this study.

Appendix B. Sloshing mode in the OWC chamber and its effect on the measured value of C_f

The instantaneous displacement at a location $\vec{x}$ inside the OWC chamber, $\zeta(\vec{x}, t)$, can be expressed as

$$\zeta(\vec{x}, t) = \Re\left(\sum_{n=1}^{N} \hat{\zeta}_n(\vec{x}) e^{-in\omega t}\right) \tag{B.1}$$

where $\Re(.)$ means taking the real part of its argument and $\hat{\zeta}_n(\vec{x})$ is the complex amplitude of the n-th harmonic waves. The cross-sectional averaged surface displacement is

$$\langle\zeta(\vec{x}, t)\rangle = \Re\left(\sum_{n=1}^{N} \left\langle\hat{\zeta}_n(\vec{x})\right\rangle e^{-in\omega t}\right) \tag{B.2}$$

where $\langle.\rangle$ means the cross-sectional average of its argument. If the k-th harmonic waves can excite a sloshing mode, then $\left\langle\hat{\zeta}_k(\vec{x})\right\rangle = 0$.

For a standalone OWC-pile of the same dimensions, Xu et al. (2016) have predicted theoretically that the first sloshing mode occurs at $L/D = 1.6633$ for $h/D = 2.32$ and $L/D = 1.7059$ for $h/D = 2.48$, respectively. This first mode of sloshing can also be validated by considering the simple relationship that the wave length of the first sloshing mode should correspond to two times the dimension of the sloshing chamber. In this case, the inner diameter of the OWC chamber is 0.119 m, the two value sof L/D above correspond to $L = 0.2079$ m and 0.2132 m, respectively; both are very close to twice the inner diameter of the chamber. These wave lengths of first sloshing mode correspond to wave periods of 0.364 s and 0.369 s, respectively. Therefore, the sloshing mode cannot be excited by the waves of fundamental frequency in our experiment, i.e., the measured $\left\langle \hat{\zeta}_1(\vec{x}) \right\rangle$ is always not influenced by sloshing modes (i.e., $\left\langle \hat{\zeta}_1(\vec{x}) \right\rangle \neq 0$) for the tested frequencies. However, the second harmonic period for $T\sqrt{g/D} = 6.20$ is 0.350 s and the third harmonic period for $T\sqrt{g/D} = 9.74$ is 0.367 s, which are very close to the aforementioned sloshing periods for the two water depths. Therefore, for $T\sqrt{g/D} = 6.20$ it is expected that $\left\langle \hat{\zeta}_2(\vec{x}) \right\rangle = 0$, and for $T\sqrt{g/D} = 9.74$ it is expected that $\left\langle \hat{\zeta}_3(\vec{x}) \right\rangle = 0$. Because the wave gauge used to measure the surface elevation inside the OWC chamber is located at 3.7 cm away from the center line, which always cause the measured $\left\langle \hat{\zeta}_2(\vec{x}) \right\rangle$ for $T\sqrt{g/D} = 6.20$ and the measured $\left\langle \hat{\zeta}_3(\vec{x}) \right\rangle$ for $T\sqrt{g/D} = 9.74$ to be larger than zero, resulting in an over-estimation of the mean velocity associated with the higher harmonic waves that excite the sloshing mode and thus an underestimation of C_f. Other higher harmonic waves periods may also excite sloshing modes of higher frequency; however, the short duration of each test run prevented them from growing to influential amplitudes.

References

Abanade, J., Greaves, D., Iglesias, G., 2014. Wave farm impact on the beach profile: A case study. Coastal Engineering 86, 36–44.

Arena, F., Romolo, A., Malara, G., Ascanelli, A., 2013. On design and building of a u-owc wave energy converter in the mediterranean sea: a case study. In: ASME 2013 32nd International Conference on Ocean, Offshore and Arctic Engineering. American Society of Mechanical Engineers, pp. 1–8.

Bingham, H. B., Ducasse, D., Nielsen, K., Read, R., 2015. Hydrodynamic analysis of oscillating water column wave energy devices. Journal of Ocean Engineering and Marine Energy 1 (4), 405–419.

Boccotti, P., 2007a. Caisson breakwaters embodying an owc with a small openingpart i: Theory. Ocean Engineering 34 (5-6), 806–819.

Boccotti, P., 2007b. Comparison between a u-owc and a conventional owc. Ocean Engineering 34 (5-6), 799–805.

Boccotti, P., Filianoti, P., Fiamma, V., Arena, F., 2007. Caisson breakwaters embodying an owc with a small openingpart ii: A small-scale field experiment. Ocean Engineering 34 (5-6), 820–841.

Bureau of Ocean Energy Management, 2017. Ocean Wave Energy. `http://www.boem.gov/Renewable-Energy-Program/Renewable-Energy-Guide/Ocean-Wave-Energy.aspx`, accessed: 2017-07-07.

Chisholm, D., 1983. Two-Phase Flow in Pipelines and Heat Exchangers. G. Godwin in association with Institution of Chemical Engineers, London, UK.

Contestabile, P., Ferrante, V., Di Lauro, E., Vicinanza, D., et al., 2016. Prototype overtopping breakwater for wave energy conversion at port of naples. In: The 26th International Ocean and Polar Engineering Conference. International Society of Offshore and Polar Engineers, pp. 616–621.

Deng, Z. Z., Huang, Z. H., Law, A. W. K., 2013. Wave power extraction by an axisymmetric oscillating-water-column converter supported by a coaxial tube-sector-shaped structure. Applied Ocean Research 42, 114–123.

Deng, Z. Z., Huang, Z. H., Law, A. W. K., 2014. Wave power extraction from a bottom-mounted oscillating water column converter with a v-shaped channel. Proceedings of the Royal Society A: Mathematical, Physical and Engineering Sciences 470, 20140074.

DNV-GL, 2007. DNV-RP-C205: Environmental conditions and environmental loads. Det Norske Veritas.

Elhanafi, A., Fleming, A., Macfarlane, G., Leong, Z., 2016a. Numerical energy balance analysis for an onshore oscillating water columnwave energy converter. Energy 116, 539–557.

Elhanafi, A., Fleming, A., Macfarlane, G., Leong, Z., 2017. Underwater geometrical impact on the hydrodynamic performance of an offshore oscillating water column-wave energy converter. Renewable Energy 105, 209–231.

Elhanafi, A., Macfarlane, G., Fleming, A., Leong, Z., 2016b. Scaling and air compressibility effects on a three-dimensional offshore stationary owc wave energy converter. Applied Energy 189, 1–20.

Evans, D., 1978. The oscillating water column wave-energy device. IMA Journal of Applied Mathematics 22, 423–433.

Evans, D., 1982. Wave-power absorption by systems of oscillating surface pressure distributions. Journal of Fluid Mechanics 114, 481–499.

Falcão, A., Gato, L., Nunes, E., 2013. A novel radial self-rectifying air turbine for use in wave energy converters. part 2. results from model testing. Renewable Energy 53, 159–164.

Falcao, A. F. O., 2000. The shoreline owc wave power plant at the azores. In: Proceedings of 4th European Wave Energy Conference. pp. 42–47.

Falnes, J., 2007. A review of wave-energy extraction. Marine Structures 4, 185–201.

Fleming, A. N., Macfarlane, G. J., 2017. Experimental flow field comparison for a series of scale model oscillating water column wave energy converters. Marine Structures 52, 108–125.

Fossa, M., Guglielmini, G., 2002. Pressure drop and void fraction profiles during horizontal flow through thin and thick orifices. Experimental Thermal and Fluid Science 26, 513–523.

Goda, Y., 1999. A comparative review on the functional forms of directional wave spectrum. Coastal Engineering Journal 41 (1), 1–20.

Goda, Y., Suzuki, T., 1976. Estimation of incident and reflected waves in random wave experiments. In: Proceedings of the 15th Conference of Coastal Engineering. ASCE, Reston, VA, USA, pp. 828–845.

Hawaii State Energy Office, 2007. State of Hawaii Energy Policy Directives. `http://energy.hawaii.gov/energypolicy`, accessed: 2017-07-07.

He, F., Huang, Z., 2017. Characteristics of orifices for modeling nonlinear power take-off in wave-flume tests of oscillating water column devices. Journal of Zhejiang University-Science A 18, 329–345.

He, F., Huang, Z. H., Law, A. W. K., 2013. An experimental study of a floating breakwater with asymmetric pneumatic chambers for wave energy extraction. Applied Energy 106, 222–231.

Henriques, J. C. C., Cndido, J. J., Pontes, M. T., Falco, A. F. O., 2013. Wave energy resource assessment for a breakwater-integrated oscillating water column plant at porto, portugal. Energys 63, 52–60.

Huang, Z. H., 2007. An experimental study of wave scattering by a vertical slotted barrier in the presence of a current. Ocean Engineering 34(5-6), 717–723.

Isaacson, M., Premasiri, S., Yang, G., 1998. Wave interactions with vertical slotted barrier. Journal of Waterway, Port, Coastal, and Ocean Engineering 124 (3), 118–126.

Iturrioz, A., Guanche, R., Lara, J. L., Vidal, C., Losada, I. J., 2015. Validation of OpenFOAM® for oscillating water column three-dimensional modeling. Ocean Engineering 107, 222–236.

Kakuno, S., Liu, P., 1993. Scattering of water waves by vertical cylinders. Journal of Waterway Port Coastal and Ocean Engineering 119, 302–322.

Koo, W., Kim, M., 2010. Nonlinear time-domain simulation of a land-based oscillating water column. Journal of waterway, port, coastal, and ocean engineering 136 (5), 276–285.

Longuet-Higgins, M. S., 1983. On the joint distribution of wave periods and amplitudes in a random wave field. Proc. R. Soc. Lond. 389, 241–258.

López, I., Andreu, J., Ceballos, S., Martnez de Alegra, I., Iigo Kortabarria, I., 2013. Review of wave energy technologies and the necessary power-equipment. Renewable and Sustainable Energy Reviews 27, 413–434.

López, I., Pereiras, B., Castro, F., Iglesias, G., 2015. Performance of owc wave energy converters: influence of turbine damping and tidal variability. International Journal of Energy Research 39 (4), 472–483.

Martins-Rivas, H., Mei, C. C., 2009. Wave power extraction from an oscillating water column at the tip of a breakwater. Journal of Fluid Mechanics 626, 395–414.

Mei, C., 1989. The Applied Dynamics of Ocean Surface Waves. World Scientific Publishing, Singapore.

Mendoza, E., Silva, R., Zanuttigh, B., Angelelli, E., Andersen, T. L., Martinelli, L., Nrgaard, J. Q. H., Ruolc, P., 2014. Beach response to wave energy converter farms acting as coastal defence. Coastal Engineering 87, 97–111.

Mustapa, M. A., Yaakob, O. B., Ahmed, Y. M., Rheem, C., Koh, K. K., 2017. Wave energy device and breakwater integration : A review. Renewable and Sustainable Energy Reviews 77 (April), 43–58.

Ning, D., Shi, J., Zou, Q., Teng, B., 2015. Investigation of hydrodynamic performance of an owc (oscillating water column) wave energy device using a fully nonlinear hobem (higher-order boundary element method). Energy 83, 177–188.

Ning, D., Wang, R., Gou, Y., Zhao, M., Teng, B., 2016a. Numerical and experimental investigation of wave dynamics on a land-fixed owc device. Energy 115, 326–337.

Ning, D., Wang, R., Zou, Q., Teng, B., 2016b. An experimental investigation of hydrodynamics of a fixed owc wave energy converter. Applied Energy 168, 636 – 648.

Sarmento, A. J. N. A., Falcao, A. F. O., 1985. Wave generation by an oscillating surface-pressure and its application in wave-energy extraction. Journal of Fluid Mechanics 150, 467–485.

Setoguchi, T., Santhakumar, S., Maeda, H., Takao, M., Kaneko, K., 2001. A review of impulse turbines for wave energy conversion. Renewable Energy 23, 261–292.

Sheehan, C., Harrington, J., 2012. An environmental and economic analysis for geotube coastal structures retaining dredge material. Resources, Conservation and Recycling 61, 91–102.

Simonetti, I., Cappietti, L., El Safti, H., Oumeraci, H., 2015. Numerical Modelling of Fixed Oscillating Water Column Wave Energy Conversion Devices: Toward Geometry Hydraulic Optimization. In: Proceedings of the ASME 2015 34th International Conference on Ocean, Offshore and Arctic Engineering. Vol. 9. pp. 1–10.

Stratigaki, V., Troch, P., Stallard, T., Forehand, D., Folley, M., Kofoed, J. P., Benoit, M., Babarit, A., Vantorre, M., Kirkegaard, J., 2015. Sea-state modification and heaving float interaction factors from physical modelling of arrays of wave energy converters. Journal of Renewable and Sustainable Energy 7, 061705.

Su, Z., 2013. Experimental study of the breakwater efficiency of a cylindrical pile model. Tech. rep., Final Year Project Report, Department of Civil and Environment Engineering, Nanyang Technological University, Singapore.

Suh, K.-D., Jung, H. Y., Pyun, C. K., 2007. Wave reflection and transmission by curtainwall–pile breakwaters using circular piles. Ocean Engineering 34 (14-15), 2100–2106.

Sundar, V., et al., 2002. Hydrodynamic pressures and forces on quadrant front face pile supported breakwater. Ocean engineering 29 (2), 193–214.

Teixeira, P. R., Davyt, D. P., Didier, E., Ramalhais, R., 2013. Numerical simulation of an oscillating water column device using acode based on Navier-Stokes equations. Energy 61, 513–530.

Torre-Enciso, Y., Ortubia, I., de Aguileta, L. L., Marqués, J., 2009. Mutriku wave power plant: from the thinking out to the reality. In: Proceedings of the 8th European wave and tidal energy conference, Uppsala, Sweden. Vol. 710. pp. 319–329.

Vicinanza, D., Nørgaard, J. H., Contestabile, P., Andersen, T. L., 2013. Wave loadings acting on overtopping breakwater for energy conversion. Journal of Coastal Research 65 (sp2), 1669–1674.

Vyzikas, T., Deshoulières, S., Barton, M., Giroux, O., Greaves, D., Simmonds, D., 2017. Experimental investigation of different geometries of fixed oscillating water column devices. Renewable Energy 104, 248–258.

Wang, R., Ning, D., Zhang, C., Zou, Q., Liu, Z., 2018. Nonlinear and viscous effects on the hydrodynamic performance of a fixed owc wave energy converter. Coastal Engineering 131, 42–50.

Xu, C. H., Huang, Z. H., Deng, Z. Z., 2016. Experimental and theoretical study of a cylindrical oscillating water column device with a quadratic power take-off model. Applied Ocean Research 57, 19–29.

Yueh, C.-Y., Chuang, S.-H., 2013. A piston-type porous wave energy converter theory. Journal of Marine Science and Technology 21 (3), 309–317.

Zhang, D., Li, W., Lin, Y., 2009. Wave energy in china: Current status and perspectives. Renewable Energy 34, 2089–2092.

Zhang, Y., Zou, Q., Greaves, D., 2012. Air-water two-phase flow modelling of hydrodynamic performance of an oscillating water column device. Renewable Energy 41, 159–170.